




Revisiting Alpert's Correlations: Numerical Exploration of Early-Stage Building Fire and Detection

Yanfu Zeng and Ho Yin Wong, Research Centre for Fire Safety Engineering, Department of Building Environment and Energy Engineering, The Hong Kong Polytechnic University, Kowloon, Hong Kong

Wojciech Węgrzyński, Fire Research Department, Building Research Institute (ITB), Filtrowa 1 St., 00-611 Warsaw, Poland

Xinyan Huang , Research Centre for Fire Safety Engineering, Department of Building Environment and Energy Engineering, The Hong Kong Polytechnic University, Kowloon, Hong Kong*

Received: 3 February 2023/**Accepted:** 27 June 2023/**Published online:** 11 July 2023

Abstract. Alpert's correlations of fire ceiling jets have been widely used in the design of heat detectors and sprinklers since the 1970s. However, these correlations are primarily derived from large fire tests of 3.8–98 MW, high ceilings, and ideal liquid spraying flames. Thus, the feasibility of Alpert's correlations for the smoke ceiling jet in early-stage fire detection with smaller fire sizes is still unclear. This study constructs a numerical model that is first validated by Alpert's original ceiling temperature and velocity data of large fire powers. Then, the numerical model further explores the feasibility of Alpert's correlations in predicting the gas temperature and velocity in steady-burning fires with 50–500 kW. Modelling confirms the accuracy of Alpert's temperature correlations for the ceiling jet region, but suggests a large uncertainty of assuming a constant turning-region temperature for early-stage fires. Moreover, the modelled velocity pattern of smoke ceiling jet in the plume region is non-uniform, and its value in the ceiling jet region is significantly higher than Alpert's fitting correlation. Finally, the response time of the heat detector and sprinkler in the ceiling jet region predicted by the numerical model is shorter than Alpert's correlations, which suggests the conventional design based on Alpert's correlations is sufficiently conservative.

Keywords: Fire simulation, Ceiling jet, Fire safety design, Fire detection, Numerical validation

Abbreviations

CFD	Computational fluid dynamics
FDS	Fire dynamics simulator
HRR	Heat release rate
HRRPUA	Heat release rate per unit area
PE	Polyethylene

*Correspondence should be addressed to: ; Xinyan Huang, E-mail: xy.huang@polyu.edu.hk



PS	Polystyrene
RTI	Response time index

Symbols

D	Effective diameter of fuel (m)
H	Ceiling height above fuel surface (m)
L_f	Mean flame height (m)
r	Radial distance to the fire centreline (m)
\dot{Q}	Heat release rate (kW)
Δt	Time interval (s)
T	Temperature ($^{\circ}\text{C}$)
V	Gas velocity (m/s)

Subscripts

g	Gas
d	Device
n	Time step

1. Introduction

In building fires, a thermal plume rises from the burning fuel due to the upward buoyancy force until it impinges on the ceiling, where it forms a horizontal flow spreading out rapidly below the ceiling surface. This type of gas flow is referred to as the ceiling jet [1]. Based on whether the flame reaches the ceiling or not, it can be further classified into two types. One is the smoke ceiling jet when the smoke plume generated from fire is obstructed by the ceiling (Fig. 1a), and the other is the flame ceiling jet when the flame is large enough to impinge the ceiling directly (Fig. 1b). Due to this flow behaviour, the fire protection products, such as sprinkler and fire (heat and smoke) detectors, are mainly installed at the ceiling level aiming for an early response. It is then essential to understand the characteristics of ceiling jet flows to improve fire protection designs and practices [2].

In the 1970s, Alpert proposed the first theoretical model of a ceiling jet to predict gas velocities, gas temperatures, and the thickness (or depth) of a steady fire-driven ceiling jet flow [3]. To confirm the theory, around 15 experiments were conducted in a very large building so that the ambient effects and the smoke descending layer formed by the fire product accumulation can be minimized [4]. The tests were performed under the horizontal and smoothed ceiling, where the depth of the beams or structures under that ceiling surface was less than 1% of the ceiling height, allowing the interruption of the structures to the ceiling jet flow to be neglected. Various fire sources and fuels were used in these tests, such as heptane spray fire and ethanol pool fire, and the ceiling height ranged from 4.6 m to 18 m. The gas temperature and velocity below the ceiling were recorded by thermocouple and hot-wire anemometers, while most of the measurements were several meters away from the fire but only few data above the fire source.

It should be noted that the heat release rates (HRR) of these tests at the steady burning stage mainly ranged from 3.8 MW to 98 MW except for one ethanol pool

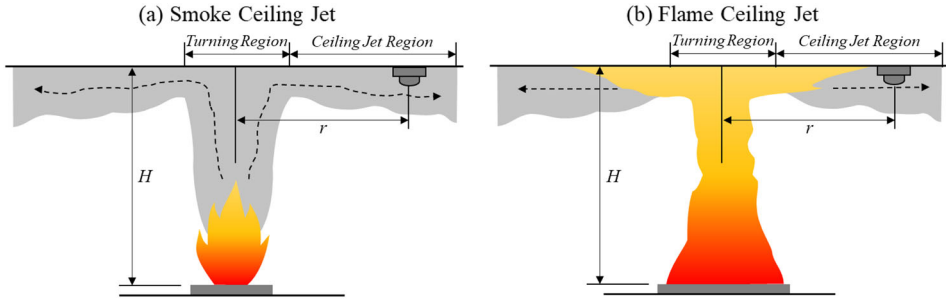


Figure 1. Ceiling jet flow below an unconfined ceiling.

Table 1
Information on Fire and Fuel in Alpert's Original Experiments in the 1970s [4, 10]

Fire source and fuel	Ceiling Height, H (m)	Fire HRR (MW)	Diameter of Fuel (m)	Cal. flame height, L_f (m)	L_f/H	Type of ceiling jet
Ethanol pool	8.61	0.62	1.09	2.0	0.23	Smoke
Cardboard boxes	13.87	3.8	2.94	3.4	0.25	Smoke
Wood pallet stack	15.54	4.4	1.38	5.4	0.34	Smoke
PE bottles in cardboard boxes	13.41	34.4	2.77	12.5	0.93	Flame/Smoke
PS jars in cardboard boxes	13.87	98.5	2.94	20.4	1.47	Flame
Heptane Spray A	7.92	7.2	3.66	4.4	0.56	Smoke
Heptane Spray B	7.92	12.5	3.66	6.5	0.82	Smoke
Heptane Spray C	7.92	17.9	3.66	8.1	1.02	Flame/Smoke
Heptane Spray D	7.92	21.5	3.66	9.0	1.13	Flame
Heptane Spray E	4.57	7.2	3.66	4.4	0.99	Flame/Smoke
Heptane Spray F	4.57	12.5	3.66	6.5	1.42	Flame
Heptane Spray G	4.57	17.9	3.66	8.1	1.77	Flame

fire of 619 kW (Table 1). Based on these experimental data, the thickness of the ceiling jet was found to be approximately 5 to 12% of the ceiling height, and semi-empirical correlations were derived, widely known as Alpert's correlations, to predict the gas temperature and velocity in the ceiling jet flow at a given position:

$$\begin{cases} T - T_\infty = 5.38 \frac{\dot{Q}^{2/3} / H^{5/3}}{(r/H)^{2/3}} & \text{for } r/H > 0.18 \\ T - T_\infty = 16.9 \dot{Q}^{2/3} / H^{5/3} & \text{for } r/H \leq 0.18 \end{cases} \quad (1)$$

$$\begin{cases} V = 0.197 \frac{(\dot{Q}/H)^{1/3}}{(r/H)^{5/6}} & \text{for } r/H > 0.15 \\ V = 0.947(\dot{Q}/H)^{1/3} & \text{for } r/H \leq 0.15 \end{cases} \quad (2)$$

where T is the gas temperature in ceiling jet flow, °C; V is the gas velocity in ceiling jet flow, m/s; T_∞ is the ambient temperature, °C; \dot{Q} is the heat release rate, kW; r is the horizontal distance to the fire centreline, m; and H is the height between ceiling and fuel surface, m.

The correlations are divided into two parts, with one part applying to the plume impinging area or turning region (Fig. 1), where the plume temperature and velocity are assumed unchanged ($r/H \leq 0.18$ for temperature prediction and $r/H \leq 0.15$ for velocity prediction). The other part applies outside of the turning region as the flow spreads away horizontally. These correlations have been widely used to estimate the response of ceiling-mounted devices [5], despite the transport time of the fire gases from the source to the detector is ignored [6]. They are also applied to predict the possible fire damage to ceiling constructions [7] and validate the numerical model for fire research [8, 9]. With the latest knowledge of the virtual origin source of fire plumes and the convective heat release rate of materials, Alpert re-analysed experimental data for five materials and introduced revised correlations in 2011 [10]. Nevertheless, the original correlations still remain popular in the fire industry due to their simplicity, while the revised ones contain more variables to consider.

To address the limitations of Alpert's correlations, such as the requirements of the smoothed ceiling, steady-state fire, and unconfined space, a wide range of research has been followed to further explore the ceiling jet behaviours. Heskestad and Hamada [11] found that, instead of using ceiling height as the normalizing length scale, an expression of plume radius could better correlate the ceiling jet excess temperature with the observation radius, while the ratio of flame height to ceiling height is within 2. Kung *et al.* [12] conducted 17 experiments with transient growing rack storage fires, which present a lower excess temperature than Heskestad's correlation. Mangs and Keski-Rahkonen [13] proposed new correlations to predict the maximum ceiling jet temperature driven by car fires. Liu *et al.* [14] studied the ceiling jet temperature in a high-altitude environment (3650 m / 64.3 Pa), which was significantly lower than the predicted values by Alpert's correlations. The impacts of sidewalls on ceiling jet behaviour have been studied inside infrastructures such as tunnels and subway stations [15, 16]. The activation time of sprinkler heads under different ceiling shapes [17] and fire growth rate [18] has been compared. Experimental data provide a much shorter response time of sprinklers in confined rooms, due to the accumulation of hot gases, compared to the predictions by Alpert's correlations [19–21].

With the development of computational models in their capability and accuracy, numerical investigation has become more popular in fire research due to its low cost and consistency [2, 9, 22, 23]. Wang *et al.* [24] use Computational Fluid Dynamics (CFD) model to validate Kawagoe's compartment fire correlations, in which the numerically predicted results, e.g., HRR and airflow rate, were well

agreed with the experimental data. Hu et al. [25] constructed the numerical model of a tunnel to investigate the gas temperature of the ceiling jet, in which the discrepancy between numerical and experimental results is less than 10%. Johansson [9] built CFD models of ceiling jet fires and proposed new correlations based on numerical results. Sirvain [26] also simulated the temperature profile of the ceiling jet for a fire of 1–4 MW. Aleksander et al. [27] and Węgrzyński et al. [28] used ANSYS Fluent to study sprinkler activation during complex compartment fires and assess the effects of natural ventilation on the activation pattern of the sprinkler. More recently, artificial intelligence models that are trained by a big numerical database have been used to predict the ceiling jet flow and fire detection time for complex floorplans [29, 30] and false ceilings [31].

Referring to Alpert's original experiments, it is noteworthy that the correlations were derived based on large fire tests. However, these correlations are now widely used for early-stage fire detection and suppression when the heat release rate is relatively low. In room-level experiments, the sprinkler with a 57–68 °C response temperature can activate with an HRR between 50 and 200 kW [32, 33], where the accumulation of hot smoke contributes to an earlier response. Even for an unconfined space with a 3.5 m ceiling height, an HRR of 180 kW is suggested to be the minimum fire size to activate a heat detector or sprinkler with 57 °C response temperature [34], while the HRR value is only 0.2% to 30% of the fire size in Alpert's original experiments. To the best of the author's knowledge, the validation of Alpert's correlations in early-stage fire has not been conducted yet, as the original experiments were based on large fire tests.

This study is to investigate whether Alpert's correlation is still applicable to low-HRR fires by using numerical experiments. In this paper, the CFD model of the ceiling jet will be first validated by reproducing Alpert's original experimental results. With the validated ceiling jet model, the feasibility of applying Alpert's correlations are verified for early-stage small fires.

2. Numerical Model of Ceiling Jet

2.1. A Brief Review of Alpert's Pioneering Tests in the 1970s

In the 1970s, Alpert conducted a series of large fire tests with various fire sources and fuels, such as heptane spray fire (major), ethanol pool fire, wood pallet fire, polyethylene (PE) and polystyrene (PS) fires, etc. (Table 1). Key features of these high-power tests are:

- (1) All experimental data used to derive empirical correlations were recorded during the steady burning period, but the fire varies with time in real scenarios, especially in the early stage.
- (2) The height of the ceiling ranges from 4.6 m to 18 m in these large fire tests, while the typical value for civil buildings is usually smaller than 3.5 m.
- (3) Most of the experimental data were measured during the high-speed spraying tests. These fires typically occur in high-pressure gas pipelines or other special-

ized equipment, which is not the representative scenario for most real building fires.

- (4) As for the steady-state HRR when data were collected, the value ranged from 3.8 MW to 98 MW except for one 619 kW ethanol pool fire. These fires are much larger than normal early-stage fires before triggering any fire detector.

The measurements from these large fire tests, together with some reduced-scale test results (ceiling heights of 0.6–1.2 m and HRRs of 5–32 kW) and theoretical analysis of buoyancy flow, form the basis of classical Alpert's physics-based empirical correlations of Eqs. (1–2).

For the experiments with large HRR compared to the space, the flame will be strong enough to directly impinge the ceiling and form a flame ceiling jet flow, resulting in a different magnitude of gas temperature compared to the smoke impingement. Heskestad et al. [35] proposed the empirical correlation to calculate flame height (L_f) based on HRR (\dot{Q}) and effective diameter of fuel (D):

$$L_f = -1.02D + 0.235\dot{Q}^{2/5} \quad (3)$$

Based on the ratio of calculated flame height to the ceiling height, it could be primarily predicted that the portions of the experiment with flame ceiling jet and smoke ceiling jet are approximately 50/50, as shown in Table 1. When the average flame height is close to the ceiling, the intermittent flame plume and smoke plume may reach the ceiling periodically, so these borderline cases ($L_f/H = 0.9$ – 1.1) are denoted as “Flame/Smoke” in the table.

In Alpert's theoretical model of the ceiling jet, the turning (or plume) region where the upward plume turns to horizontal flow below the ceiling is assumed with an unchanged velocity magnitude [1]. The plume temperature and velocity above the fire source are assumed independent of radius, and only one temperature measurement was placed in the turning region in the larger fire tests as a flat line. For tests using heptane spray fuel, only temperature data in Heptane Spray G was presented. Other measurements were placed in the ceiling jet region, and most of them were positioned at least 4.6 m away from the fire centreline, as shown in Fig. 2. However, the current sprinkler or fire detectors design usually has a spacing of 3 to 6 m [36, 37], while the maximum radial distance between fire point and the device would be around 2 to 3 m. This means the gas temperature in the near-fire region is more important for the prediction of device response, while the experimental data here are relatively few.

2.2. Numerical Experiments

CFD model was built using Fire Dynamics Simulator (FDS) version 6.7.7 and validated by reproducing four literature experiments: Ethanol Pool test, Heptane Spray C, Heptane Spray E, and Heptane Spray G (Table 1). These experiments were chosen because the detailed test information was well specified in the literature as well as the experimental data presented [10] so that the uncertainties of the computational setting can be minimized. The fuels of ethanol and heptane spray

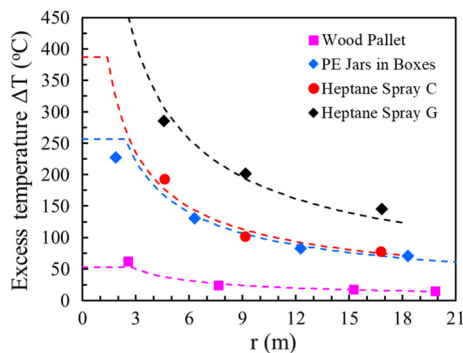


Figure 2. Temperature measurements in some ceiling jet experiments [10], while marks indicate experimental data and dash lines are the predicted temperature profiles by Alpert's correlations.

**Table 2
The Computational Setting of Numerical Ceiling Jet Model**

Attributes	Ethanol pool	Heptane spray C	Heptane spray E	Heptane spray G
Size of fire source	1.0 × 1.0 m ²	3.6 m diameter circle with 8 spray nozzles		
HRRPUA or fuel flowrate	0.62 MW/m ²	38.1 L/min	15.2 L/min	38.1 L/min
Heat of combustion (MJ/kJ)	25.6	41.2	41.2	41.2
Chemical HRR (MW)	0.62	17.8	7.2	17.8
Radiative fraction	0.26	0.33	0.33	0.33
Convective HRR (MW)	0.46	12.0	4.8	12.0
Ceiling height (m)	8.6	7.9	4.6	4.6
Calculated flame height (m)	2.0	8.1	4.4	8.1
Simulated flame height (m)	2.6 ± 0.1	Reach ceiling	Reach ceiling	Reach ceiling

are also better representations of steady-state fire. These four experiments cover different fire sources, ceiling heights, HRRs, and types of ceiling jet flow (flame and smoke ceiling jet). Thus, the reliability and accuracy of the numerical model can be maximized.

The computational settings of each experimental scenario are summarized in Table 2. The default settings of the FDS are used and any change of the default settings will be specified. The setting of HRR and ceiling height follow the provided information from the literature. For the fire source of the ethanol pool test, a 1 × 1 m² burner vent is placed on the floor, while the surface temperature is 300 °C and the heat release rate per unit area (HRRPUA) is 619 kW/m². The ramp-up time of the HRR is set as 1 s so that the fire can quickly reach a steady state. For heptane spraying tests, the fire source setup covers three parts: nozzle setup, flow setup and fuel property. Eight spray nozzles are evenly positioned at the perimeter of a circle with a 3.6 m diameter. The nozzles are placed one mesh above the floor to avoid possible interruptions to the fuel spraying. The spraying orientation of nozzles is set toward the centre of the circle and at an angle of 45°

from the ground. Flow velocity is 10 m/s and flow ramp-up time is 1 s. The total flow rates of the fuel from 8 nozzles for Test C and G are 38.1 L/min, while 15.2 L/min for Test E. As suggested by Alpert [10], the heat of combustion is 25.6 MJ/kg for ethanol and 41.2 MJ/kg for heptane. The radiative fraction of ethanol and heptane is 0.26 and 0.33, respectively.

For the boundary conditions, the properties of the ceiling and floor are set as default inertia to represent a smooth surface, and four vertical boundaries are set as ‘OPEN’ surface property which connects to the environment in order to reproduce the unconfined experimental space. The environmental temperature is set as 26.7 °C based on the literature [4]. The turbulence model uses the Large Eddy Simulation (LES), the radiation is solved by the Optically-Thin model, and fire extinction is controlled by both critical flame temperature and oxygen concentration.

While the ceiling jet flows symmetrically from the fire centreline, the gas properties are similar in each direction. Therefore, to save computational resources and speed up the simulation, a restricted domain is proposed when considering the computational domain. While the full domain means the domain is extended from the fire source to the distance beyond the furthest experimental measurement of each experiment at four directions and represents a box shape, the restricted domain is extended with this distance only in the positive x-direction. The extensions to the other directions will be the distance of the ceiling height and finally represent a rectangle shape, as shown in Fig. 3. Figure 4a compares temperature profiles for the Heptane Spray E test between the restricted and the full domains, where the modelling results are almost the same.

The mesh resolution has an impact on the simulation result, while a better resolution of the calculation can be achieved with more mesh cells [38]. A mesh sensitivity study was conducted for the Ethanol Pool test (0.62 MW) to find an acceptable minimum mesh size. As shown in Fig. 4b, the reduction of mesh size from 0.1 m to 0.05 m has a limited influence on the temperature profile. Thus, 0.1 m is considered the most cost-effective setup, so it is used for all modelling scenarios.

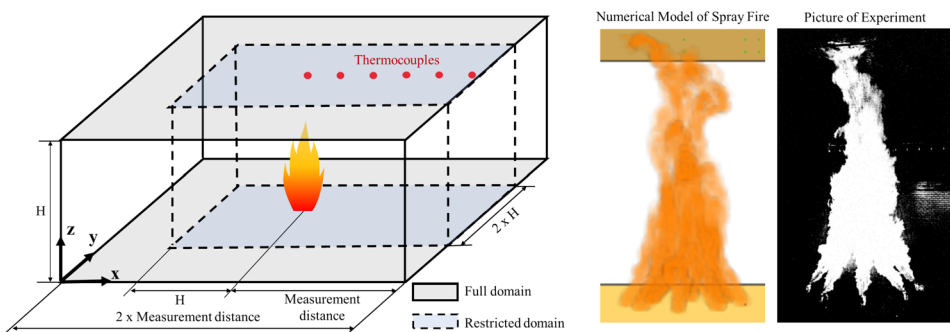


Figure 3. Simulation domain of the experimental scenario and the comparison between numerical model and experiment picture of high-speed spray fire (see more details in Video 1–4).

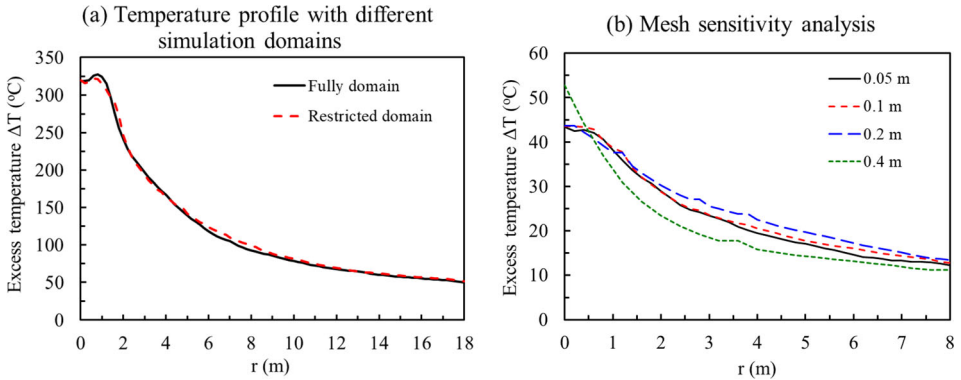


Figure 4. Temperature profiles impacted by (a) simulation domain and (b) mesh size.

For the data collection, at the levels of 0.1 m and 0.2 m below the ceiling, temperature and velocity measurements are made with every 0.2 m horizontal distance at positive x -direction. The height of measurements is about 1–4% of the room height below the ceiling, so it can be regarded within the ceiling jet flow [4]. The bead diameter of the thermocouple is 1.0 mm, and the gas velocity result is recorded with both total velocity and U -velocity (velocity at x -direction). A gas phase device tree is set in the fire centreline with an interval of 0.1 m to quantify the ‘Heat Release Rate per Unit Length’, which is the result obtained by performing integration of the heat release rate per unit volume over two horizontal axes, in order to record the flame length [38]. 2-D slices of gas temperature and velocity are set at the y -axis across the centre of the fire source to visualize the field distribution. Output interval is set as 1 s. Due to the turbulent nature of the fire, the temperature reading at the same position has a maximum of 5% difference at various times. To minimize this difference, all the presented results are the average value of a 20 s continuous period during the steady burning state.

3. Model Validation Results

3.1. Validated Ceiling Gas Temperature Distribution

Figure 5 presents the temperature profile with radial distance. The measurement height is 0.2 m below the ceiling (2–4% of the ceiling height). Simulation videos are also provided with the flame motion and temperature/velocity 2-D slices across the fire centre. Before the comparison between experimental data, fitting correlation, and numerical simulations, the definition of accuracy shall be clarified:

- 1) Fire is a very complex phenomenon, so all fire tests and measurements have large uncertainties inherently. Especially large-scale fire experiments have an

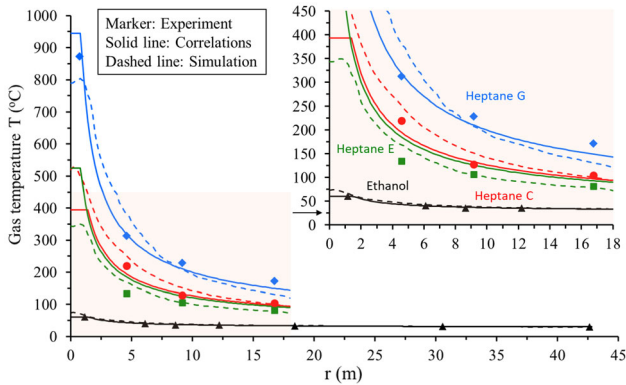


Figure 5. Temperature profiles with the position in different experimental scenarios, while the markers indicate experimental data, the solid lines present the fitting results by Alpert's correlations, and the dash lines are the predicted results by the numerical model.

Table 3
Average Temperature Differences Between Experiment, Alpert's Correlations, and Numerical Model

Comparison	Turning region (%)	Ceiling jet region (%)
Experiment and Numerical model (0.6–17.9 MW)	11*	15
Experiment and Alpert's correlations (0.6–17.9 MW)	5*	12
Numerical model and Alpert's correlations (0.6–17.9 MW)	28	14
Numerical model and Alpert's correlations (0.2–0.5 MW)	18	8

* In the turning region, there are only two experimental data from Ethanol and Heptane Spray G tests

uncertainty of at least 10–30%. Alpert's papers only presented the average temperature and velocity without giving error bars [3];

- Alpert's correlation is a fitting of experimental data, so the discrepancies due to fitting must exist. As shown in Fig. 5, clear deviations can be found between fitting lines by Alpert's correlations (solid line) and experimental data points (markers). The average fitting error is about 12%, which cannot be ignored when compared with numerical simulations later.

Figure 5 also compares the predicted temperature result by the numerical model (dash line) and experimental data: in the ceiling jet region ($r/H > 0.18$), a good agreement can be found between simulated and measured results, and the average difference is around 15% (Table 3), which is comparable to the fitting uncertainty

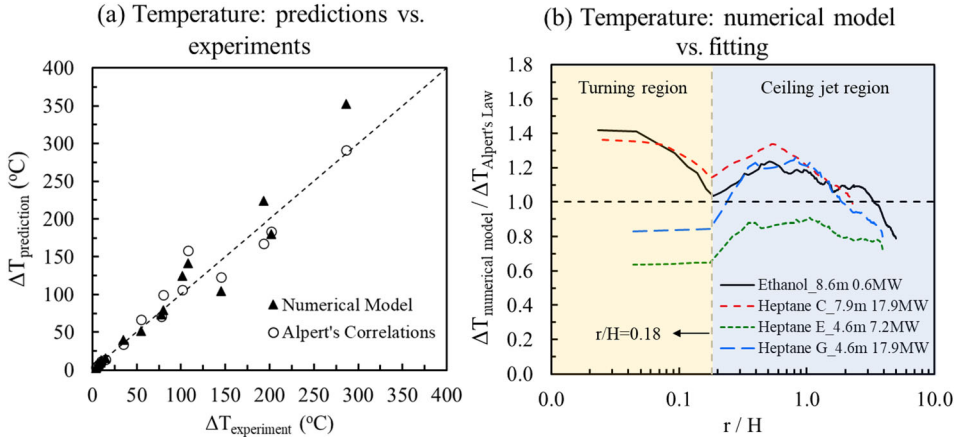


Figure 6. Comparisons of temperature result in experimental scenarios by (a) numerical model with experiment and Alpert's correlations with experiments; (b) numerical model with Alpert's correlations.

of the Alpert's correlations. For the Heptane Spray E scenario, the predicted results by the numerical model are even closer to the measurements than fitting by Alpert's correlations.

Figure 6a further compares the differences between measured results with fitted and simulated results. In general, the two methods present similar discrepancies compared to the experimental result. Figure 6b presents the ratio of predicted results by the numerical model to Alpert's correlations in different regions, where both the fitting correlation and numerical model can predict the experiments well in the ceiling jet region. Specifically, the error of the numerical model, 15%, is also comparable to that of fitting by Alpert's empirical correlations, which is about 12% in Table 3. Considering the large uncertainty in experimental data, the numerical model is sufficiently accurate.

For the turning (plume) region ($r/H \leq 0.18$), only the experimental data for the Ethanol and Heptane Spray G fire tests are reported [10]. For both experiments, only one measurement has been made in this area, so the temperature distribution cannot be verified. The difference between the numerical prediction and experiments is 11%, which is very promising. On the other hand, the average difference between the numerical model and Alpert's correlations rises to 28% in this area (Table 3). Among the four scenarios, the Heptane G case with a strong flame ceiling jet can still have good agreement between fitting and simulated results, as shown in Fig. 6b. However, in other cases, the discrepancy keeps increasing with the decrease of radial distance in the turning region with a maximum difference of 40%. It raises a more detailed observation of the fire behaviour in the turning region by comparing the temperature.

Figure 5 shows that in the scenario of Ethanol and Heptane Spray E, the temperature profiles present a continuous raising trend in the turning region, different

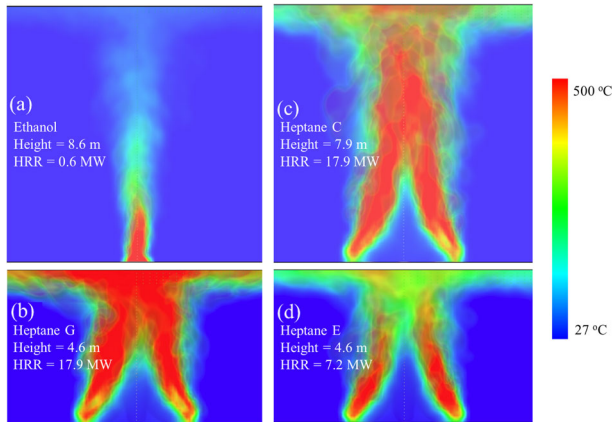


Figure 7. Temperature fields in the simulation of (a) Ethanol Pool with smoke ceiling jet; (b) Heptane Spray G with flame ceiling jet, (c) Heptane Spray C with flame/smoke ceiling jet; and (d) Heptane Spray E with flame/smoke ceiling jet (averaged over 20 s, see more details in Video S1).

from the uniform profile assumed by Alpert's correlations. A similar observation is also found for modelling fire of 1–4 MW in [26]. Figure 7 presents the 20-s average temperature fields of each experimental scenario (see the detailed comparison in Video S1). It shows that the type of fire source (pool fire or spray fire) significantly affects the flame shape.

In pool fires, the flame is driven by the upward buoyancy force and the air entrainment flow towards the fire from the surroundings. Thus, the fire plume is concentrated on the centre of the fuel bed, as shown in Fig. 7a. As for the flame formed by the high-speed spraying of liquid fuel, the initial injecting momentum governs the formation of flame shape. Since the flames are from multiple separated nozzles, the overall shape is rather dispersed (Fig. 7b and d). With the increase of the ceiling height, however, the injecting momentum gradually loses, and the surrounding air entrainment flow pushes the individual flames to the centre leading to the flame merge at high elevation (Fig. 7c). It explains the discrepancies in temperature profiles in the turning region.

On the other hand, the type of ceiling jet (i.e., the ratio of flame height and ceiling height) also influences the temperature distribution in the turning region. In the scenario of Heptane Spray G (Fig. 7b), the flame height is much greater than the ceiling height ($L_f/H = 1.77$), and the turning region is fully occupied by the flame. Thus, the temperature distribution tends to be unchanged.

As for the scenarios of Heptane Spray C (Fig. 7c) and Heptane Spray E (Fig. 7d), although they are both at near-ceiling conditions ($L_f/H \sim 1.0$), the flames generated from nozzles in Heptane Spray C have already concentrated on the centre, resulting in a raising temperature profile in the turning region. For the Heptane Spray E jet flame in Fig. 7d, instead of merging to the centre, the spray-

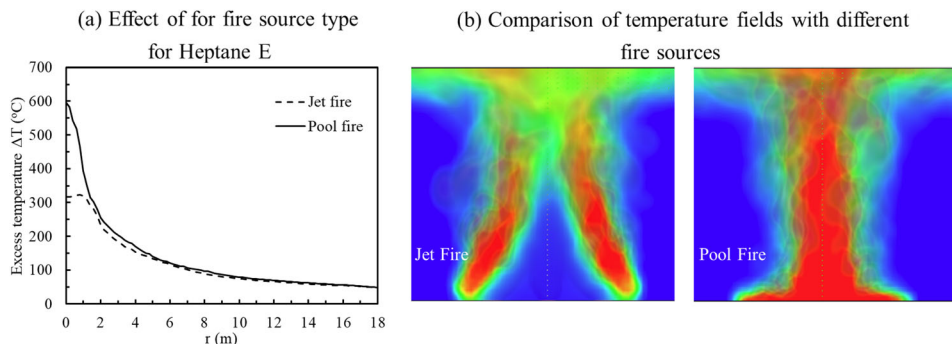


Figure 8. Temperature distribution between liquid fuel spray and pool fire (Heptane Spray E), (a) temperature profile and (b) temperature field (averaged over 20 s).

ing flames still maintain separately due to the low ceiling height and large buoyancy flow.

To further demonstrate the effect of fire source type on temperature distribution in the turning region, an additional scenario was built based on Heptane Spray E while changing the fire source to pool fire. Figure 8a presents the comparison of temperature profiles between different fire source types. The pool fire produces a changing magnitude of temperature in the turning region while the jet fire remains stable, while the average difference is 69%. It can be explained by the temperature fields while pool fire is concentrated in the centre and jet fire is separated, as shown in Fig. 8b. Based on the above simulation results, the simple assumption of an unchanged temperature field in the turning region might not be reasonable for all fire scenarios, and it could be affected by many factors, including the fire source (i.e. flow momentum) and type of ceiling jet (i.e. relationship between flame height and ceiling height). To fully explore the critical situation of the temperature profile change, more simulation works are required as well as verification by the real fire experiments. In general, the current numerical model can well predict the temperature in Alpert's classical experiments.

3.2. Validated Ceiling Velocity Profile

The experimental velocity measurements are mainly from large growing fire tests (e.g., wood pallet fire) and lab-scale tests [10]. It is noteworthy that the uncertainty of velocity measurement inside the hot turbulent flame or smoke jet is very large, even under today's measurement technics. Among the four selected experimental scenarios, only the Ethanol Pool fire test and Heptane Spray C test were reported with velocity measurements, and only one measurement was made in the turning region. We record both total velocity and U-velocity (velocity at x-direction) in simulations and found that they have the same up-and-down pattern. Especially in the ceiling jet region, the total velocity and U-velocity readings are almost the same, as the bulk flow is essentially horizontal. In the turning region where the flow transits from vertical to horizontal, U-velocity has a smaller read-

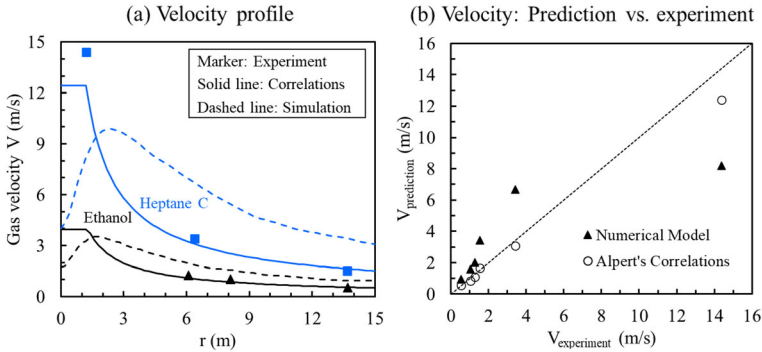


Figure 9. Velocity profiles with the position in different experimental scenarios.

Table 4
Average Velocity Differences Between Experiment, Alpert's Correlations and Numerical Simulation

Comparison	Turning region (%)	Ceiling jet region (%)
Experiment and Numerical model (0.6–17.9 MW)	47*	61
Experiment and Alpert's correlations (0.6–17.9 MW)	14*	11
Numerical simulation and Alpert's correlations (0.6–17.9 MW)	47	63
Numerical simulation and Alpert's correlations (200–500 kW)	42	66

*In the turning region, there are only one experimental data from the Heptane Spray G test

ing than total velocity, especially near the fire centreline. To accurately predict the response of the sprinkler/detector in the further step, the total flow velocity should be considered as the appropriate indicator experienced by the device. Therefore, the total velocity results are reported in the following sections.

Figure 9 compares the velocity results between the experiment (markers), Alpert's correlations (solid lines), and simulation (dash lines). In the ceiling jet region, a significant discrepancy can be found between experimental measurement and predicted gas velocity by the numerical model, while the predicted gas velocity is higher than measured. Table 4 summarized the differences between the experiment, empirical fitting and numerical model, where the average difference between the experiment and simulation is 61%. As for Alpert's fitting correlation, the average difference to the measurements (solid line) is 11% far from the fire centreline.

As for the turning region, a different trend can be observed in simulated results when approaching the fire centreline, as shown in Fig. 9a. Instead of being unchanged as assumed by Alpert's correlations, the numerical model predicts that

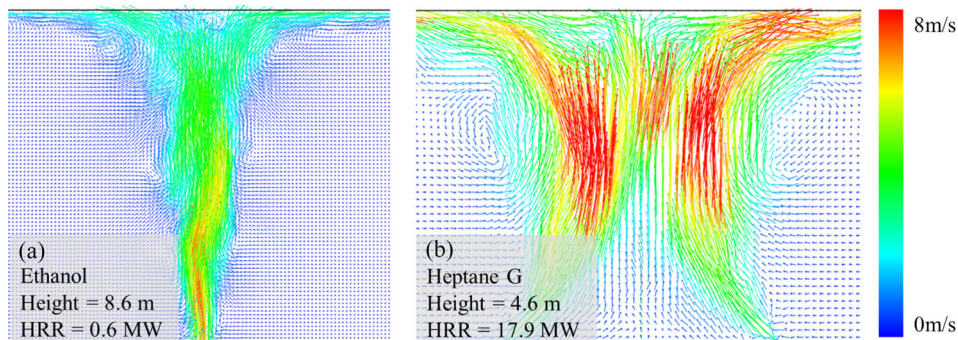


Figure 10. Velocity fields of experimental scenario: (a) ethanol pool with smoke ceiling jet; (b) Heptane Spray C with flame/smoke ceiling jet (see more details in Video S2).

the velocity right above the fire source centre is very low. It increases with radial distance to a maximum value at about 2 m away from the fire centreline. Figure 9b further demonstrates the discrepancies (about 47%) between simulated and experimental results. Note that the experimental measurement of gas velocity is very challenging, especially when the flame is impinging the ceiling. In other words, these experimental data should have a large uncertainty, so engineers should be very cautious about the test data rather than believing them blindly.

Figure 10 presents the velocity fields of two experiments with vectors. See the detailed comparison in Video S2. The turning region is where the vertical plume transfers to horizontal flow, and in both simulation scenarios, gas velocity suffers a dissipation at the plume/ceiling intersection, especially in the centre of the fuel bed. This explains the low value of velocity in the centre area. However, it still requires more experimental measurements to verify this finding. In general, the velocity predicted by the numerical model is larger than the experimental measurements in the ceiling jet region, while presenting a decreasing trend when approaching the fire centreline.

4. Feasibility of Alpert's Correlations in Early-Stage Fire Scenario

4.1. Establishment of the Typical Early-Stage Fire Scenario

To verify the feasibility of applying Alpert's correlations in the early fire stage, fire scenarios with relatively low-HRRs are modelled to compensate for Alpert's large fire experiments. Two ceiling heights, 2.5 m and 3.5 m, were selected to cover the typical room height of a normal building. Fires with five different HRRs were modelled with both ceiling heights: 50, 100, 200, 300, and 500 kW. Ethanol Pool fire is modelled by setting the burner vent as the fire source. HRRPUA is set as 500 kW/m² and the burner area is determined accordingly, except for the 200-kW fire which is set as 416.7 kW/m² in order to align the mesh boundary and set up a

near-square burner. The mesh size is reduced to 2.5 cm for 50–300 kW simulations and 5 cm for 300–500 kW simulations to adjust the reduction of HRR. A restricted simulation domain is applied where the extension in the positive x-direction is 10 m. Other computational settings are the same as previously validated ones.

4.2. Predicted Ceiling Gas Temperature

For these small fires, the measurement height of gas temperature and velocity is set to 0.05 m and 0.1 m below the ceiling (2–3% of ceiling height) for 2.5 m and 3.5 m ceiling height respectively, which is consistent with the measurement height ratio in previous model validation scenarios. Figure 11a presents the temperature field of the scenario with 2.5 m height and 500 kW HRR, and Video S3 presents simulation results for all scenarios. Figure 12 presents the temperature profiles with radial distance with three different HRRs. In the ceiling jet region, the simulated result agrees well with Alpert's fitting correlation, showing only an 8% average difference (see summary in Table 3). Despite this good agreement, it should be noted that there is potentially a more significant discrepancy if the correlation is used to predict a growing fire situation. One of the possible reasons is that heat losses to the ceiling might be larger at the growing stage when the ceiling has not been fully heated up yet.

As for the turning region, the temperature keeps increasing when approaching the fire centreline instead of being constant, and the maximum temperature is also 18% higher than the calculations. This phenomenon is the same as what has been found in the experimental scenario of Ethanol and Heptane Spray E in Fig. 5. Thus, for the fire with a relatively small HRR, the simple assumption of uniform temperature distribution in the turning region becomes questionable.

Figure 13 presents the temperature ratio of the numerical model to Alpert's fitting correlation, and the results concentrate on the 1.0 ± 0.2 in both the turning region and ceiling jet region. Based on the above results, it can be concluded that

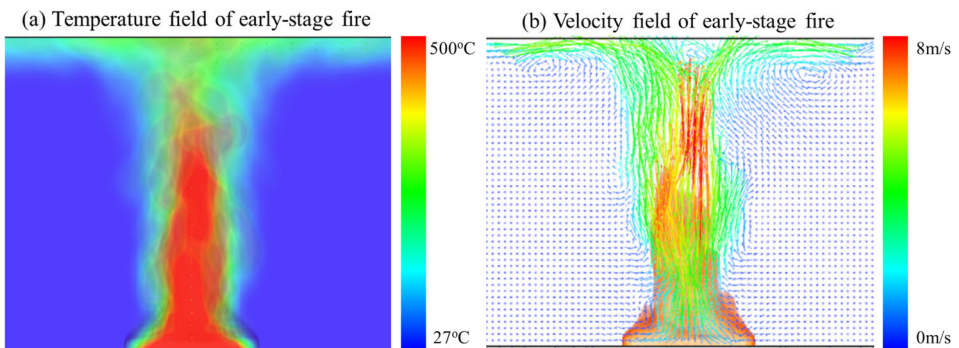


Figure 11. Numerical predicted fields of early-stage fire scenarios with 2.5 m height and 500 kW: (a) temperature field (average over 20 s), and (b) velocity field (see more details in Video S3-4).

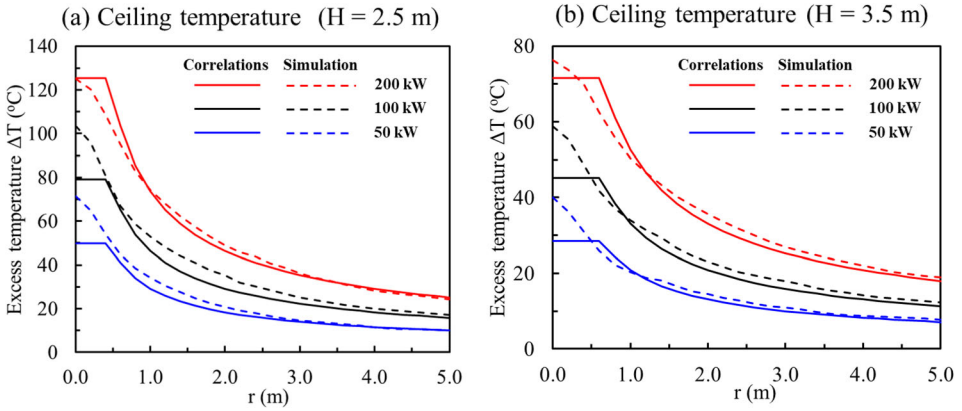


Figure 12. Temperature profiles of early-stage fire scenarios with a ceiling height of (a) 2.5 m and (b) 3.5 m.

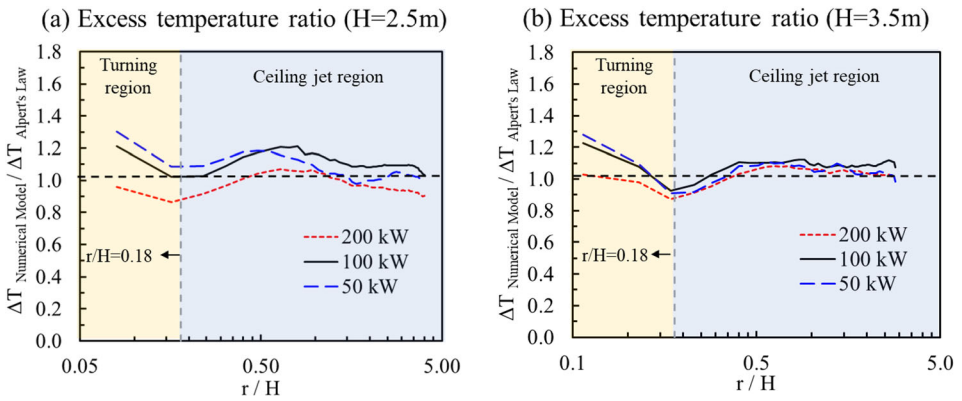


Figure 13. The excess temperature ratio in early-stage fires with a ceiling height of (a) 2.5 m and (b) 3.5 m.

for early-stage fires with smaller HRR, Alpert's fitting correlation can still well predict the gas temperature in the ceiling jet region, while it might underestimate the temperature in the turning region. It should also be noted that the effect of burner shape is not explored in this study, which could possibly affect the flame height and subsequently change the temperature profile in the turning region.

4.3. Predicted Ceiling Velocity Profiles

Figure 11b presents the velocity field with vector in an early-stage fire scenario with 2.5 m and 500 kW, where the velocity dissipation can be observed right above the fire centre. Figure 14 shows the horizontal velocity profiles with radial distance. The same pattern with previous experimental scenarios has been found here, where the model predicted velocity is 66% higher than the fitting value in

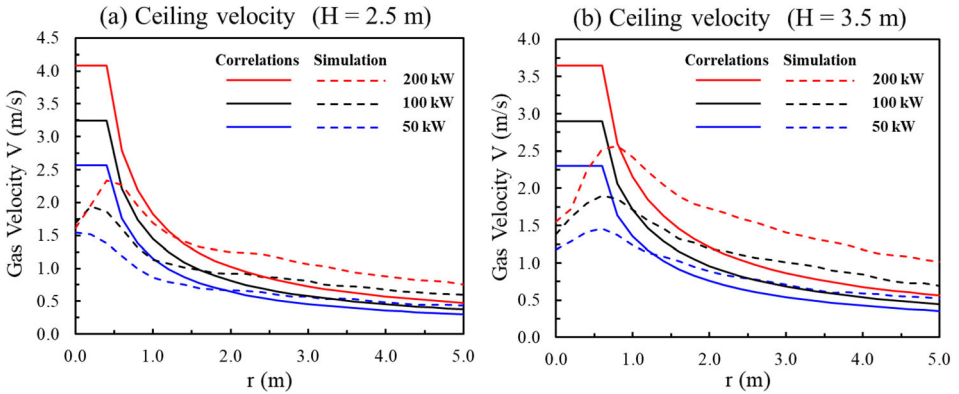


Figure 14. Velocity profiles of early-stage fire scenarios with a ceiling height of (a) 2.5 m and (b) 3.5 m.

the ceiling jet region and suggests a decreasing trend when approaching the fire centreline in the turning region with 42% discrepancies compared to Alpert's fitting correlation (Table 4).

5. Prediction of Sprinkler/Detector Response

The most important application of Alpert's correlations is to predict the thermal response of ceiling-mounted devices, i.e., sprinklers and heat detectors, where the area is large enough to neglect the accumulation of smoke layer [39]. Schiffliti et al. [6] have introduced the procedures to model the response of fire protection devices to fires, where Alpert's correlations is applied to calculate the temperature and velocity of fire gases in ceiling jet, and Eq. 4 to analyze the temperature change of the device:

$$\Delta T_d = T_{d,n} - T_{d,n-1} = \frac{V_n^{1/2} (T_{g,n} - T_{d,n-1})}{RTI} \Delta t \quad (4)$$

where ΔT_d is the temperature rise of the device, °C; $T_{d,n}$ is the device temperature at time step n , °C; $T_{d,n-1}$ is the device temperature at time step $(n-1)$, °C; V_n is the gas velocity at time step n , m/s; $T_{g,n}$ is the gas temperature at time step n , m/s; RTI is the response time index of the device, $m^{1/2} \cdot s^{1/2}$; and Δt is the time interval, s.

The predictions of the sprinkler activation time have been made for early-stage fire scenarios with an RTI of $80 m^{1/2} \cdot s^{1/2}$ and an activation temperature of $57^\circ C$, which are standard values of the sprinkler. It should be noted that the RTI is actually found to be not constant under low gas velocity situations, as conductive losses to sprinkler fittings could no longer be neglected [40]. Since the goal of this work is to demonstrate the discrepancies between Alpert's correlations and the proposed numerical model instead of providing an accurate prediction of the device, constant RTI is exercised to simplify the calculations. Figure 15 shows the

predictions of activation time against radial distance by Alpert's correlations and numerical model. It can be observed that in the near-fire region, the numerical model suggests a slower response of sprinklers than Alpert's correlations.

Although the temperature prediction by the numerical model is higher in this area, the predicted velocity is significantly lower than the value by Alpert's correlations, which results in a longer response time. With the increase of radial distance, however, the predicted response time by the numerical model increases faster than the fitting value by Alpert's correlations. This is because the temperature predictions by the two methods are very similar in this region, while the higher prediction of gas velocity by the numerical model can accelerate the activation of the device.

Figure 16 presents the analysis of activation time against HRR in both the turning region and ceiling jet region. For the analysis of the turning region, the sprinkler is assumed to be mounted 0.2 m away from the fire centreline. For the analysis of the ceiling jet region, a prescriptive design case that complies with the Chinese fire code is proposed [41], where the maximum spacing of sprinklers is 3.6 m for the high-rise civil building, e.g., office buildings and hotels. Thus, the maximum horizontal distance between the fire centre and the sprinkler is 2.6 m. As shown in Fig. 16a, due to the high temperature above the fire source, the sprinklers activated very soon, which suggests that the minimum HRR to activate a sprinkler can be as low as 25 kW with a ceiling height of 2.5 m by Alpert's correlations. Meanwhile, the delay of the sprinkler activation mainly occurred with high HRR, while the average difference in activation time in this region is 42%.

Figure 16b presents the response predictions in the ceiling jet region, where the response time is much longer and the calculated minimum HRR to activate the device raises to 140 kW. It should be noted that the calculations based on Alpert's correlations neglect the time required for the transport of the fire gases from the source to the detector [6], which is successfully reproduced by the numerical

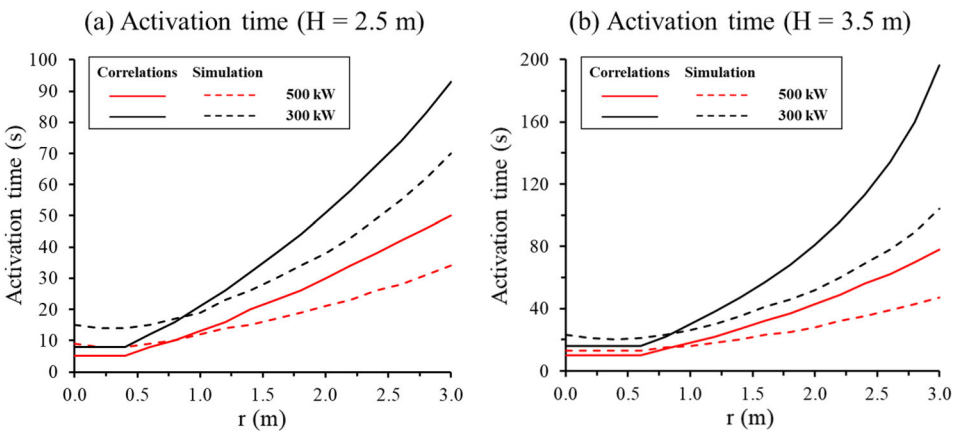


Figure 15. Predicted activation time against radial distance with a ceiling height of (a) 2.5 m and (b) 3.5 m.

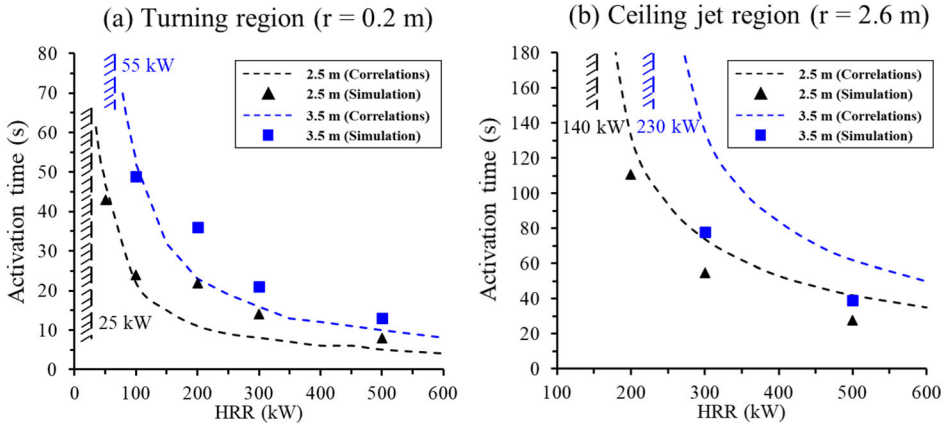


Figure 16. Predicted device activation time against HRR in (a) turning region and (b) ceiling jet region.

model. It spends around 11 to 17 s for the ceiling jet gas temperature and 4 to 7 s for the velocity to raise from the ambient value to a stable state at the 2.6 m radial distance. Nevertheless, the numerical predicted activation time is 31% quicker compared to the fitted result outside the plume region due to higher simulated gas velocity at the steady period.

In general, the numerical model suggests a slower response of the sprinkler/detector in the turning region and quicker sprinkler activation in the ceiling jet region. In the design of the sprinkler system, the engineers prefer the worst design fire scenario in which the fire source is as far as possible from the sprinklers. Hence the calculations are normally done based on the analysis of the ceiling jet region. While a safety margin of 20% to 50% is commonly exercised in design practices, in this case, the design based on Alpert's correlations is sufficiently conservative.

6. Conclusions

This study built the numerical model of a ceiling jet, which was validated by four large fire experiments (0.6–17.9 MW). The result shows the predicted temperature profiles by the numerical model have good agreement with the experimental measurements, while the average difference is 11% in the turning region and 15% in the ceiling jet region. This difference is similar to the difference between experiments and fitting correlation, which is 5% in the turning region and 12% in the ceiling jet region. It means the numerical model can predict the gas temperature of the ceiling jet accurately. Meanwhile, the numerical model shows both the fire source setup and ceiling jet type will affect the temperature field in the turning region. Thus, the simple assumption of unchanged gas temperature in the turning region by Alpert's correlations might not be reasonable for all fire scenarios. As for the velocity result, the prediction of the numerical model is 61% higher than

the experimental measurement in the ceiling jet region, while it presents a decreasing trend when approaching the fire centreline due to velocity dissipation at the plume/ceiling intersection, with 47% difference compared to the predicted value by Alpert's correlations.

This study further investigates typical early-stage fire scenarios with ceiling heights ranging from 2.5 to 3.5 m and constant HRRs ranging from 50 to 500 kW. The temperature result shows the discrepancy between predictions by Alpert's correlations and the numerical model is 8% in the ceiling jet region, and the temperature profiles in the turning region present a clear decreasing trend with radial distance, which suggests a possible under-estimation on the gas temperature by Alpert's correlations in near fire field. The velocity result for early-stage fires presents the same pattern as previous large fire tests, where the modelled value is 42% lower in the turning region and 66% higher in the ceiling jet region compared to the fitted value.

Modelling results show that the predicted sprinkler response time by the numerical model is 31% faster in the ceiling jet region. Thus, the current sprinkler system design based on Alpert's ceiling jet correlation is considered to be sufficiently conservative, while the proposed CFD model is encouraged to be applied to investigate ceiling jet characteristics in near-fire region. To further verify the findings in this study, detailed experimental measurements should be followed, especially in the turning region, so that revised models can be proposed to better describe the ceiling jet behaviour in early-stage fires.

Acknowledgements

This work is funded by the Hong Kong Research Grants Council Theme-based Research Scheme (T22-505/19-N) and the PolyU Emerging Frontier Area (EFA) Scheme of RISUD (P0013879). The authors thank Dr R. L. Alpert for valuable information on his pioneering tests and discussions.

Declarations

Conflict of interest The authors declare that they have no known competing financial interests or personal relationships that could have appeared to influence the work reported in this paper.

SUPPLEMENTARY INFORMATION

The online version contains supplementary material available at <https://doi.org/10.1007/s10694-023-01461-0>.

References

1. Alpert RL (2016) Ceiling Jet Flows. In: Hurley MJ (ed) SFPE Handbook of Fire Protection Engineering Springer, New York, pp 429–454
2. Khetata MS (2016) Numerical Prediction of Thermal and Dynamic Characteristics of a Fire-Induced Ceiling-Jet. Polytechnic Institute of Bragança (Master Thesis), [online]. <https://www.proquest.com/openview/cc353e8998964ab7eb98942cd56126f9/1?pq-origsite=gscholar&cbl=2026366&diss=y>. (Accessed 10 July 2023)
3. Alpert RL (1975) Turbulent ceiling-jet induced by large-scale fires. *Combust Sci Technol* 11:197–213. <https://doi.org/10.1080/00102207508946699>
4. Alpert RL (1972) Calculation of response time of ceiling-mounted fire detectors. *Fire Technol* 8:181–195. <https://doi.org/10.1007/BF02590543>
5. Evans DD, Stroup DW (1986) Methods to calculate the response time of heat and smoke detectors installed below large unobstructed ceilings. *Fire Technol* 22:54–65. <https://doi.org/10.1007/BF01040244>
6. Schifiliti RP, Custer RLP, Meacham BJ (2016) Design of Detection Systems. In: Hurley MJ (ed) SFPE Handbook of Fire Protection Engineering Springer, New York, pp 1314–1377
7. Alpert RL, Ward EJ (1984) Evaluation of unsprinklered fire hazards. *Fire Saf J* 7:127–143. [https://doi.org/10.1016/0379-7112\(84\)90033-X](https://doi.org/10.1016/0379-7112(84)90033-X)
8. van der Heijden MGM, Loomans MGLC, Lemaire AD, Hensen JLM (2013) Fire safety assessment of semi-open car parks based on validated CFD simulations. *Build Simul* 6:385–394. <https://doi.org/10.1007/s12273-013-0118-7>
9. Johansson N, Wahlqvist J, Van Hees P (2015) Numerical experiments in fire science: a study of ceiling jets. *Fire Mater* 39:533–544. <https://doi.org/10.1002/fam.2253>
10. Alpert RL (2011) The Fire-Induced Ceiling-Jet Revisited. In: The Science of Suppression, Proceedings of Fireseat 2011 at the National Museum of Scotland. The University of Edinburgh, Scotland, Edinburgh, pp 1–21, [online]. <https://www.fireseat.eng.ed.ac.uk/sites/fireseat.eng.ed.ac.uk/files/images/FS11-Proc-Alpert.pdf>. (Accessed 10 July 2023)
11. Heskestad G, Hamada T (1993) Ceiling jets of strong fire plumes. *Fire Saf J* 21:69–82. [https://doi.org/10.1016/0379-7112\(93\)90005-B](https://doi.org/10.1016/0379-7112(93)90005-B)
12. Kung HC, You HZ, Spaulding RD (1988) Ceiling flows of growing rack storage fires. *Symposium (International) on Combustion* 21:121–128. [https://doi.org/10.1016/S0082-0784\(88\)80238-8](https://doi.org/10.1016/S0082-0784(88)80238-8)
13. Mangs J, Keski-Rahkonen O (1994) Characterization of the fire behaviour of a burning passenger car. Part II: parametrization of measured rate of heat release curves. *Fire Saf J* 23:37–49. [https://doi.org/10.1016/0379-7112\(94\)90060-4](https://doi.org/10.1016/0379-7112(94)90060-4)
14. Liu J, Zhou Z, Wang J et al (2018) The maximum excess temperature of fire-induced smoke flow beneath an unconfined ceiling at high altitude. *Therm Sci* 2018:2961–2970. <https://doi.org/10.2298/TSCI170926075L>
15. Ji J, Zhong W, Li KY et al (2011) A simplified calculation method on maximum smoke temperature under the ceiling in subway station fires. *Tunn Undergr Space Technol* 26:490–496. <https://doi.org/10.1016/j.tust.2011.02.001>
16. Tang F, Cao Z, Palacios A, Wang Q (2018) A study on the maximum temperature of ceiling jet induced by rectangular-source fires in a tunnel using ceiling smoke extraction. *Int J Therm Sci* 127:329–334. <https://doi.org/10.1016/j.ijthermalsci.2018.02.001>
17. Runefors M, Boström P, Almgren E (2018) Comparison of sprinkler activation times under flat and corrugated metal deck ceiling. *J Phys Confer Ser* . <https://doi.org/10.1088/1742-6596/1107/6/062006>

18. Toldra R (2023) Automatic fire sprinkler activation time with quadratic fire growth. *Fire Technol* . <https://doi.org/10.1007/s10694-023-01441-4>
19. Wade C, Spearpoint M, Bittern A, Tsai KWH (2007) Assessing the sprinkler activation predictive capability of the BRANZFIRE fire model. *Fire Technol* 43:175–193. <https://doi.org/10.1007/s10694-007-0009-5>
20. Johansson N (2018) A case study of far-field temperatures in progressing fires. *J Phys Confer Ser* . <https://doi.org/10.1088/1742-6596/1107/4/042018>
21. U.S. Nuclear Regulatory Commission (2016) NUREG-1824: verification and validation of selected fire models for nuclear power plant. Washington, [online]. <https://www.nrc.gov/reading-rm/doc-collections/nuregs/staff/sr1824/s1/index.html>. (Accessed 10 July 2023)
22. Hara T, Kato S (2006) Numerical simulation of fire plume-induced ceiling jets using the standard k- ϵ model. *Fire Technol* 42:131–160. <https://doi.org/10.1007/s10694-006-7504-y>
23. Johansson N (2014) Numerical experiments and compartment fires. *Fire Sci Rev* 3:1–12. <https://doi.org/10.1186/s40038-014-0002-2>
24. Wang Z, Zhang T, Huang X (2022) Numerical modeling of compartment fires: ventilation characteristics and limitation of Kawagoe's Law. *Fire Technol* . <https://doi.org/10.1007/s10694-022-01218-1>
25. Hu LH, Huo R, Peng W et al (2006) On the maximum smoke temperature under the ceiling in tunnel fires. *Tunn Undergr Space Technol* 21:650–655. <https://doi.org/10.1016/j.tust.2005.10.003>
26. Sirvain H (2013) Characterisation of the far field temperature under the ceiling in the Travelling Fires framework. Ghent University (Master Thesis)
27. Król A, Jahn W, Krajewski G et al (2022) A study on the reliability of modeling of thermocouple response and sprinkler activation during compartment fires. *Buildings* . <https://doi.org/10.3390/buildings12010077>
28. Węgrzyński W, Krajewski G, Tofiło P et al (2020) 3D mapping of the sprinkler activation time. *Energies* 13:1–15. <https://doi.org/10.3390/en13061450>
29. Zeng Y, Huang X (2023) Smart building fire safety design driven by artificial intelligence. In: Naser MZ (ed) *Interpretable machine learning for the analysis, design, assessment, and informed decision making for civil infrastructure* Elsevier, New York
30. Zeng Y, Li Y, Du P, Huang X (2023) GAN-driven smart fire detection analysis in complex building floorplans. *J Build Eng* (under review)
31. Khan A, Zhang T, Huang X, Usmani A (2023) Machine learning driven smart fire safety design of false ceiling and emergency machine. *Process Saf Environ Protect* (under review)
32. Madrzykowski D (2008) Impact of a Residential Sprinkler on the Heat Release Rate of a Christmas Tree Fire. Gaithersburg, MD, [online]. <https://brandveiligwonen.org/wp-content/uploads/2021/03/20080500-Madrzykowski-NIST-Impact-of-a-Residential-Sprinkler-on-christmas-tree.pdf>. (Accessed 10 July 2023)
33. Bittern A (2004) Analysis of FDS Predicted Sprinkler Activation Times with Experiments. University of Canterbury (Master Thesis), [online]. <https://ir.canterbury.ac.nz/handle/10092/14748>. (Accessed 10 July 2023)
34. Motevalli V, Yuan ZP (2008) Steady state ceiling jet behavior under an unconfined ceiling with beams. *Fire Technol* 44:97–112. <https://doi.org/10.1007/s10694-007-0027-3>
35. Heskestad G, Huang X (2016) Smart building fire safety design driven by artificial intelligence. In: Hurley MJ (ed) *SFPE handbook of fire protection engineering* Springer, New York, pp 396–428
36. Standards New Zealand (2003) NZS 4541: automatic fire sprinkler systems. Wellington

37. British Standard Institution (BSI) (2021) BS 9251-2021: fire sprinkler systems for domestic and residential occupancies. Code of practice. BSI
38. McGrattan K, McDermott R, Vanella M, et al (2021) Fire Dynamics Simulator Users Guide, 6th ed. National Institute of Standards and Technology, Gaithersburg, MD, USA
39. Deal S (1995) Technical Reference Guide for FPEtool Version 3.2. National Institute of Standards and Technology, Gaithersburg, MD, [online]. <https://www.scss.tcd.ie/Alexis.Donnelly/cedfsp/fpetool/FPETool.PDF>. (Accessed 10 July 2023)
40. Pepi JS (1986) Design characteristics of quick response sprinklers. Society of Fire Protection Engineers,
41. Ministry of Housing and Urban-Rural Development of the People's Republic China (2017) GB 50084-2017: Code for design of sprinkler systems. Ministry of Housing and Urban-Rural Development of The People's Republic China

Publisher's Note Springer Nature remains neutral with regard to jurisdictional claims in published maps and institutional affiliations.

Springer Nature or its licensor (e.g. a society or other partner) holds exclusive rights to this article under a publishing agreement with the author(s) or other rightsholder(s); author self-archiving of the accepted manuscript version of this article is solely governed by the terms of such publishing agreement and applicable law.